

Boundary-driven many-body phase transitions in a non-Hermitian disordered fermionic chain

Kuldeep Suthar

Department of Physics, Central University of Rajasthan, Ajmer - 305817, India

(Dated: February 7, 2025)

The non-Hermitian systems exhibit extreme sensitivity to the boundary conditions. The change in the eigen-spectrum with tuning boundary parameter is intimately connected to the non-Hermitian skin effect. The single-particle systems are affected by the boundary perturbations; however the interplay of a random disorder potential and non-reciprocal hopping under boundary perturbations of an interacting many-body system is not yet clear. In this work, we examine the boundary sensitivity of a non-Hermitian interacting fermionic system in the presence of a random disorder potential. A non-zero boundary parameter results in real-complex spectral transitions with non-reciprocal (or unidirectional) hopping at weak disorder. While the many-body localization at strong disorder washes away real-complex transitions leading to dynamical stability and real eigenvalue spectrum. We show that the boundary-driven real-complex spectral transitions of the non-Hermitian chain are accompanied by the corresponding changes in the level statistics and nearest level-spacing distributions. The intriguing features of non-reciprocity and boundary sensitivity are further revealed using the averaged inverse participation ratios. Finally, we find distinct behaviour in the quench dynamics of local particle density, population imbalance, and entanglement entropy of charge-density-wave ordered state that corroborate the real-complex and localization transitions. Our results provide a route to understanding disordered many-body systems under a generalized boundary.

I. INTRODUCTION

The investigations of the physical properties and topological phases of non-Hermitian systems have gained significant attention in recent years [1–6]. These systems are non-conservative in which the inherent gain or loss emerges due to coupling with external environments [7, 8]. The rapid technical advances in the ultracold atomic gases [9–14], electrical circuits [15, 16], and photonic [17–20] and acoustic systems [20–22] provide ideal platform to realize the novel phenomena in experiments. Moreover, the absence of thermalization in isolated disordered interacting Hermitian system can result in a phenomenon dubbed as *many-body localization* (MBL) [23–25]. The successful attempts to engineer the controllable environment pave a way to explore the effects of the inevitable environment on the localization properties of interacting disordered systems. These advancements provide an opportunity to discover new classes of transitions beyond the realm of Hermitian critical phenomena.

In the absence of hermiticity, the eigenspectrum of the system could be complex, which leads to many intriguing phenomena in non-Hermitian systems. One of the remarkable phenomenon is the *non-Hermitian skin effect* (NHSE) [26] which refers to an anomalous localization of extensive eigenmodes at the boundaries. Recently, the non-Hermitian Hamiltonians with dissipations and non-reciprocal hopping have been realized in experiments [9, 11, 12, 27], where the characteristic signature of NHSE and topological phenomena, including geometry-dependent [28] and high-order NHSE [29] have been observed in experiments. The existence of NHSE signals the breakdown of bulk-boundary correspondence [30–32]. The energy spectrum becomes highly sensitive to the boundary conditions as the open boundary condition (OBC) and periodic boundary condition (PBC) show distinct features. Various versions of NHSE have recently been proposed [33–38]. Previous studies on the boundary sensitivity primarily dealt with the level of single-particle systems

and revealed the interplay of system size and boundary perturbations on the existence of NHSE. The NHSE can exist even beyond OBC when one of the hopping terms is absent [39]. In recent times, the role of many-body correlations on the properties of non-Hermitian systems, including the nontrivial topology [40], relaxation dynamics [41], and entanglement transition [42, 43], have been examined. However, the investigations of NHSE for interacting disordered systems are limited. The non-Hermitian many-body localization in disordered [44–46], quasiperiodic [47–49], and electric-field-driven stark potential [50, 51] have been proposed. The two localization phenomena, NHSE and MBL, of the non-Hermitian interacting chain can be distinguished by the eigenstate properties and non-equilibrium quench dynamics [48]. Despite several theoretical investigations on non-Hermitian systems, the role of the boundary perturbations under the presence of random disorder potential for interacting non-Hermitian fermionic systems is yet to be examined.

In the present work, we explore the boundary sensitivity in the emergence of real-complex spectral and localization transitions of a many-body non-Hermitian disordered chain. Here, the spectral transition refers to the real-complex transition of the eigenenergies by a change in the boundary parameter or disorder strength in a single fermionic chain. The coupling between the two end sites of the chain is controlled by a boundary parameter. We first examine the eigenvalue spectra due to an interplay of hopping with boundary parameters in a one-dimensional interacting chain subjected to a random disorder. We find that the real-complex transitions are accompanied by localization transitions. The localization properties of the system are examined using the inverse participation ratio and nearest-neighbour level statistics. We demonstrate that the non-reciprocal hopping results in the coexistence of real-complex and localization transitions, and non-Hermitian many-body localization at strong disorder dynamically stabilizes the system. Further, we perform the quench dynamics of a density-wave ordered initial state and analyze

the disorder-averaged local particle density, occupancy imbalance, and the entanglement entropy. The localization of particles at the chain boundaries is characterized by the time-dynamics of particle density and imbalance, and entanglement entropy signals the signature of many-body localization in the non-reciprocal (and reciprocal) lattice with boundary tuning parameter.

The rest of this paper is organized as follows: Section II introduces the Hatano-Nelson model with variable boundary terms. In Section III, we discuss the real-complex transition, level statistics, inverse participation ratio, and quench dynamics of dynamical observables. Finally, the findings are summarized in Section IV.

II. MODEL HAMILTONIAN

We consider a one-dimensional Hatano-Nelson chain [52–54] of interacting fermionic atoms loaded in a random disorder potential with generalized boundary conditions. The model Hamiltonian of the system is

$$\hat{H} = - \sum_{j=1}^{L-1} \left(J_L \hat{c}_j^\dagger \hat{c}_{j+1} + J_R \hat{c}_{j+1}^\dagger \hat{c}_j \right) + \delta_R \hat{c}_1^\dagger \hat{c}_L + \delta_L \hat{c}_L^\dagger \hat{c}_1 + V \sum_j \hat{n}_j \hat{n}_{j+1} + \sum_j \epsilon_j \hat{n}_j. \quad (1)$$

Here, j represents the spatial lattice index and L is the number of lattice sites, $J_{L(R)}$ denotes the left (right)-hopping amplitude for neighbouring lattice sites, δ_L and δ_R determine generalized boundary conditions, $V > 0$ is a repulsive coulomb interaction strength between two spinless fermions at adjacent sites, and ϵ_j is a random disorder potential chosen between $[-W, W]$ with W being the disorder strength. Here, we have considered $\delta_L = \delta_R = \delta$ in the present work. In the absence of a disorder potential, the single-particle limit of the model displays a system-size dependent boundary effects and real-complex transitions of eigenspectra [39]. For $V = W = 0$, the eigenvalue equation corresponding to the above Hamiltonian is $\hat{H}_{\text{sp}} |\Psi\rangle = E_{\text{sp}} |\Psi\rangle$, where the eigenstate $|\Psi\rangle = \sum_j \psi_j |j\rangle$ with $|j\rangle = \hat{c}_j^\dagger |0\rangle$ and \hat{H}_{sp} is a single-particle Hamiltonian corresponding to Eq. (1). The solutions of the eigenvalue equation are related by the following relation [39]

$$\sin[(L+1)\theta] - \xi_1 \sin[(L-1)\theta] - \xi_2 \sin[\theta] = 0, \quad (2)$$

where $\xi_2 = (\delta_L/J_L)(J_R/J_L)^{-L/2} + (\delta_R/J_R)(J_R/J_L)^{L/2}$ and $\xi_1 = (\delta_L \delta_R / J_L J_R)$. The solutions θ of the above equation depends on hopping amplitudes and boundary terms through ξ_1 and ξ_2 , and can in general possess both real and complex values. Once the boundary terms are finite, the solutions of the equations become highly sensitive to the system size. The finite NHSE can exist when the ratio of boundary term to one of the hopping amplitudes (δ_L/J_L) (at fixed (δ_R/J_R)) is smaller than ≈ 0.07 with $J_L \neq J_R$. In case of open chain with $\delta_L = \delta_R = 0$, which leads to

$\xi_1 = \xi_2 = 0$, and the above Eq. (2) gives L real solutions $\theta = j\pi/(L+1)$. Consequently, the eigenvalues of the system are real, and the eigenstates take the form $\Psi = (r \sin[\theta], r^2 \sin[2\theta], \dots, r^L \sin[L\theta])^T$, where $r = \sqrt{J_R/J_L}$. Moreover, at higher ratios of δ to hopping amplitudes, the skin effect vanishes, and the eigenspectrum of the system exhibits a real-complex transition. It is important to note that the above model Hamiltonian [Eq. (1)] possesses real-complex transitions as it respects the time-reversal symmetry [44, 45]. We discuss in the next section the numerical results of real-complex and non-Hermitian localization transitions in the presence of a disorder potential.

III. RESULTS AND DISCUSSIONS

In this section, we first discuss our numerical results of static properties such as real-complex transitions of eigenenergies, and diagnostics of localization and extended character followed by dynamical properties. To reveal the interplay of non-hermiticity and boundary sensitivity, we consider the generalized boundary conditions on non-reciprocal couplings and numerically study the effects of random disorder potential. In the present study, the on-site interaction strength is fixed at $V = 1$ and half-filling case is considered. The static and dynamical properties are primarily examined for the system size $L = 16$.

A. Real-complex transition of eigenenergies

We first study the boundary effects on the complex energy spectra as a function of the disorder potential strength. Various regimes can be distinguished based on the fraction of the complex energies averaged over several disorder realizations. The fraction of the complex energies is defined as $f_{\text{im}} = \overline{D_{\text{im}}}/\overline{D}$ [44, 45, 47], where D_{im} is the number of eigenenergies whose imaginary part $|\text{Im}\{E\}| \geq C$ with a cutoff $C = 10^{-13}$, which is identified as the error in our numerical diagonalization. Here, E is the complex eigenenergies and D is the total number of eigenenergies. The overline denotes the average over several disorder samples.

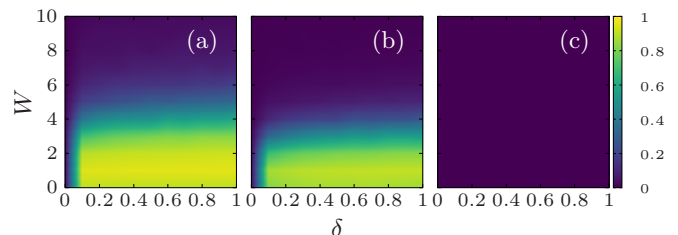


FIG. 1. The disorder-averaged complex energy fraction as a function of boundary parameter and disorder strength. Here J_L is varied to reveal the non-reciprocal coupling effects with $J_R = 1$. (a) $J_L = 0.0$, (b) $J_L = 0.5$, and (c) $J_L = 1.0$. The system size is $L = 12$. The fraction shown is averaged over 300 disorder realizations.

The spectrum of the non-Hermitian many-body lattice model [Eq. (1)] shows strong sensitivity to the boundary parameter. For a single-particle clean system, the eigen-spectrum describes a loop in the complex energy plane as δ increases. The region of complex loop structured energy spectra enhances as L increases while the real spectra region becomes narrow [39], which is consistent with the analytical solutions of Eq. (2). For many-body clean systems, the spectrum follows that of larger single-particle systems. Moreover, it is important to note that the single-particle eigenstates get delocalized (at the band center) due to pinning of the flux lines in the presence of non-reciprocal hoppings. The random disorder potential leads to a statistically symmetric spectrum in the complex plane and localizes the eigenstates. Thus, the uncorrelated disorder results in a real spectrum even for single-particle systems [52–55]. Fig. 1 shows f_{im} as a function of the boundary parameter δ and disorder strength W . The value of f_{im} is averaged over several disorder realizations in the presence of random disorder. We set one of the hoppings $J_R = 1$. First, we examine the energy spectrum for unidirectional (non-reciprocal) hopping case in which $J_L = 0$ [Fig. 1(a)], where $f_{\text{im}} = 0$ and $f_{\text{im}} = 1$ represents completely real and complex spectrum. At $\delta = 0$, the model corresponds to an open chain and can be mapped to a Hermitian system through imaginary gauge transformation [45, 55]. This results in a real spectrum that remains valid even with finite disorder. Once a finite value of δ , a link connecting both ends of the boundary, is introduced the generalized boundary leads to complex spectrum at weak disorder. This is evident from a sharp change in f_{im} at the boundary for $\delta = 0$ and $\delta = 0.1$. As W increases, the f_{im} lowers and finally becomes zero (real spectrum) at a critical disorder strength. The distributions of the eigenenergy spectrum suggest that the critical W increases as δ approaches one. The strong disorder suppresses the imaginary parts of the complex energies and dynamically stabilizes the system [44, 45]. The genesis of the realness of the spectrum lies at the single-particle level.

We further find that non-reciprocal hopping with $J_L = 0.5$ exhibits a similar eigenenergy spectrum; however, the complex energy regime is reduced. Hence, the critical W of complex-real transition depends on the difference of hopping in left and right directions. Once both hoppings are equal which turn into the Hermitian limit, the $\delta - W$ plane possess real spectrum. This demonstrates the boundary sensitivity is applicable for systems with non-reciprocal hopping.

B. Inverse participation ratio

We now examine the localization properties of the non-Hermitian systems induced by hopping anisotropy and random disorder potential. To this end, we compute the disorder-averaged inverse participation ratio (IPR) [56, 57]. It is worth noting that for non-Hermitian systems, the IPR can be defined in two ways: (i) for the right (left) eigenstates of the model Hamiltonian \hat{H} (\hat{H}^\dagger) and (ii) for the biorthogonal basis using both right and left eigenstates [58]. The disorder-averaged IPR of the n th right eigenstate and biorthogonal eigenstates

are

$$I_n = \frac{\sum_i \overline{|\phi_i^{(s,n)}|^2}}{(\sum_i \overline{|\phi_i^{(s,n)}|})^2}; \quad I_{nB} = \frac{\sum_i \overline{|\tilde{\phi}_i^{(s,n)}|^2}}{(\sum_i \overline{|\tilde{\phi}_i^{(s,n)}|})^2}, \quad (3)$$

where the overline indicates the average over disorder realizations with corresponding index s , $\phi_i^{(s,n)} \equiv (\langle n|b_i \rangle_s^*) \langle n|b_i \rangle_s$ and $\tilde{\phi}_i^{(s,n)} \equiv (\langle \tilde{n}|b_i \rangle_s^*) \langle n|b_i \rangle_s$ with n and \tilde{n} are the right and corresponding left eigenstates, and $|b_i \rangle$ are Fock space basis. The mean IPR $\bar{I} = \sum_n I_n / D_H$ and mean biorthogonal IPR $\bar{I}_B = \sum_n I_{nB} / D_H$ are obtained by averaging over the whole energy spectrum. Here, D_H is the dimension of the Hilbert space of many-body Hamiltonian. For localized states, IPR approaches a finite value (unity) while it approaches zero for delocalized states in the thermodynamic limit. The biorthogonal IPR includes the nonorthogonality of different eigenstates, thus captures the non-Hermitian effects of interacting disordered systems [45, 59].

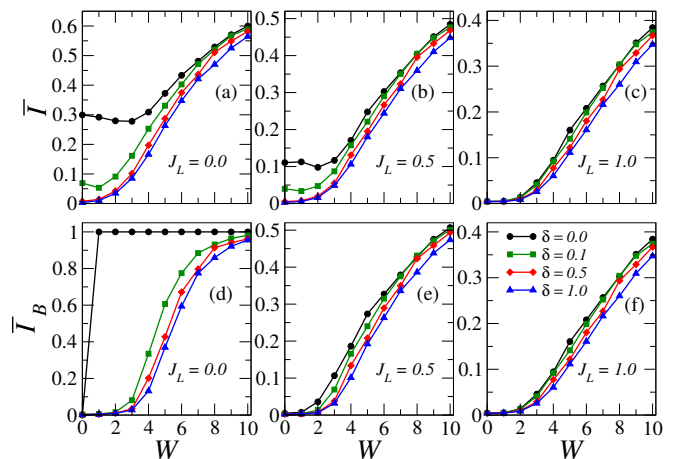


FIG. 2. The disorder-averaged IPR and the biorthogonal IPR for system size $L = 12$. (a,d) The non-reciprocal case with unidirectional hopping $J_L = 0$, (b,e) The non-reciprocal case with $J_L = 0.5$, and (c,f) $J_L = 1$ corresponds to the Hermitian limit. The upper (a,b,c) and lower (d,e,f) panel shows IPR and biorthogonal IPR, respectively. The black, green, red, and blue colored lines represent the cases with boundary parameters $\delta = 0, 0.1, 0.5$, and 1 , respectively. The IPR values are obtained by averaging the energy spectrum. Here, $J_R = 1$ and data is averaged over 300 disorder realizations.

In the unidirectional hopping ($J_L = 0$), Fig. 2(a,d) shows the \bar{I} and \bar{I}_B as a function of W for various boundary parameter values. At $\delta = 0$ (OBC), the \bar{I} is finite at weak disorder, suggesting the existence of non-Hermitian skin effect where the bulk states tend to localize at one end of a one-dimensional chain. \bar{I} further increases with enhancement in the disorder strength W . The corresponding \bar{I}_B approaches unity at an infinitesimal W . Since the degree of non-hermiticity is largest in the unidirectional hopping case, the \bar{I}_B remains one, and the NHSE dominates over the disorder-induced localization. At the finite value $\delta = 0.1$, the weak link of the ends lowers the \bar{I} value (compared to the OBC case); however, it remains finite. At higher boundary coupling strength $\delta = 0.5$,

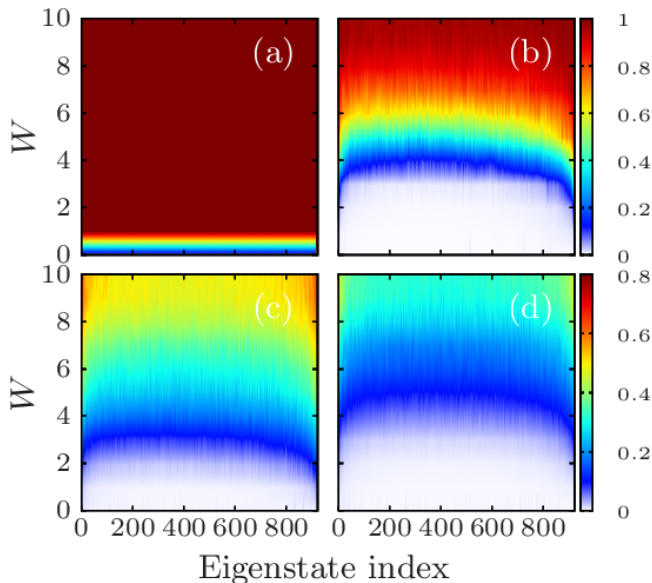


FIG. 3. The disorder-averaged biorthogonal IPR in the whole energy spectrum as a function of W for system size $L = 12$. Some specific cases are considered: (a) for unidirectional hopping with OBC ($\delta = 0$) case of generalized boundary, (b) for unidirectional hopping with $\delta = 0.5$, (c) $J_L = 0.5$ with OBC, and (d) $J_L = \delta = 1$ corresponding to Hermitian limit with PBC. The spectrum of biorthogonal IPR is averaged over 100 disorder realizations.

the \bar{I} becomes zero at lower strength W and increases with W , similar to the behaviour depicted at $\delta = 1$ (PBC). For later three cases (except OBC), the biorthogonal IPR \bar{I}_B is smaller (larger) at weak (strong) disorder strengths compared to \bar{I} . The biorthogonal IPR as a function of W in the whole energy spectrum under the open boundary condition i.e. $\delta = 0$ is shown in Fig. 3(a). The I_{nB} of all eigenstates becomes one, demonstrating the localization due to the interplay of skin effect and random disorder. Fig. 3(b) shows I_{nB} at $\delta = 0.5$ and $J_L = 0$. With finite δ , the delocalized regime appears as the skin-localization is suppressed and the gradual increase in the value of I_{nB} with W exhibits the disorder-driven localization.

For the non-reciprocal case with $J_L = 0.5$, the values of IPR and biorthogonal IPR shown in Fig. 2(b,e) indicates that the localization is sensitive to δ values. In particular, at smaller W , the \bar{I} is higher due to skin effect induced localization. Moreover, the steady \bar{I} in this case is lower than Fig. 2(a) as in the later case the unidirectional hopping promotes the skin-localization. At strong W , the apparent distinctions between the behaviour of both IPRs disappear as the degree of non-hermiticity reduces. This is also evident from the distributions of I_{nB} shown in Fig. 3(c) at $\delta = 0$ [cf. Fig. 3(b)]. Finally, in the Hermitian limit $J_L = J_R = 1$, both IPRs overlap as Hermitian systems do not show boundary sensitivity and are free from NHSE. The increase in IPRs represents the initially extended states get localized by the growing disorder. This behaviour for the Hermitian system is depicted in Fig. 2(c,f). The distinct localization of eigenstates solely due to disorder potential is presented in Fig. 3(d).

Next we turn to study the localizations using biorthogonal

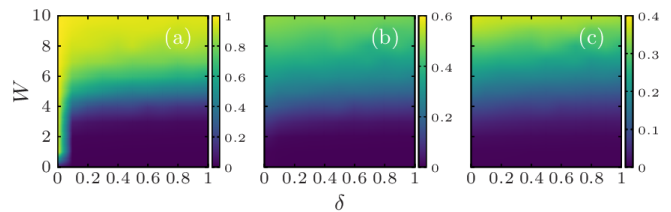


FIG. 4. The biorthogonal IPR is a function of boundary parameter and disorder strength. Here $J_R = 1$ and J_L is varied to have effects from non-reciprocal coupling to the Hermitian limit. (a) $J_L = 0$, (b) $J_L = 0.5$, and (c) $J_L = 1.0$. The values of IPR are obtained by averaging over 300 disorder realizations.

IPR as a function of δ and W . The averaged I_{nB} for three cases: unidirectional, non-reciprocal, and reciprocal hoppings are shown in Fig. 4. At $J_L = 0$, when $\delta = 0$, the particles tend to localize at one end and thus leads to finite I_{nB} (unity) even at smaller disorder strengths [Fig. 4(a)]. This behaviour is consistent with Fig. 2(a). The introduction of a small link or finite δ departs from the OBC case, and thus I_{nB} gradually increases with W and becomes unity. On the contrary, for a nonzero left hopping as shown in Fig. 4(b), the I_{nB} is zero at smaller disorder strengths for $\delta = 0$. In Hermitian limit at $J_L = 1$, the value of I_{nB} lowers at strong disorder as the localization is due to the disorder potential, and NHSE does not contribute.

C. Level statistics

We now proceed to study the level statistics of the complex energy spectrum to understand the localization properties corresponding to the real-complex transitions of the model [60–62]. We consider the nearest-level spacing $d_{1,i} \equiv \min_j |E_i - E_j|$ which defines the minimum (nearest-neighbour) distance between two eigenenergies E_i and E_j in the complex plane. We employ the unfolding procedure of the complex and real energy spectrums to obtain the nearest-neighbour distance [63–65]. The local mean density of the energy eigenvalues is

$$\bar{\rho}_i = n / (\pi d_{n,i}^2), \quad (4)$$

where n is chosen to be very small compared to the Hamiltonian matrix size and sufficiently larger than one (approximately 30). $d_{n,i}$ is the n th nearest-neighbour distance from E_i . After removing the dependence of local density on the level spacing, the rescaled nearest-neighbour distance is

$$s_i = d_{1,i} \sqrt{\bar{\rho}_i}. \quad (5)$$

The probability distribution of $\{s_i\}$ denoted as $P(s)$ is plotted in Fig. 5 for $\delta = 0$ and $\delta = 0.5$ at weak disorder, and $\delta = 0.5$ at strong disorder. With non-reciprocal hopping, at $\delta = 0$ and $W = 1$, the system is in the delocalized phase with real energy spectrum and the level-spacing distribution approaches the distribution of Gaussian orthogonal ensemble (GOE) [66],

which is given by

$$P_{\text{GOE}}^{\text{R}}(s) = \frac{\pi s}{2} \exp\left(\frac{-\pi s^2}{4}\right). \quad (6)$$

The corresponding distribution is presented in Fig. 5(a) for non-reciprocal hoppings, $J_L = 0.5$ and $J_R = 1$. Note that at weak disorder with $\delta = 0$, both IPR and biorthogonal IPR differ in values, and the later is zero as it is not suffered from NHSE (cf. Fig. 2(b)). As discussed earlier, an infinitesimal boundary coupling leads to a real-complex transition at weak disorder strengths. This transition results in to change in the distributions from that of GOE to the Ginibre ensemble [62, 63, 66, 67]. As an illustration, for $\delta = 0.5$ and $W = 1$, the

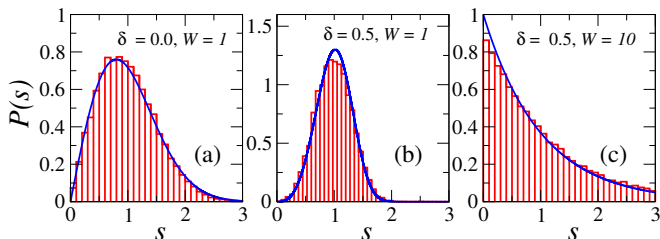


FIG. 5. The level-spacing distributions for non-reciprocal hopping strengths lead to non-hermiticity of the system. (a,b) At weak disorder, the boundary coupling exhibits a transition of nearest level-spacing distribution from GOE to Ginibre distribution, corresponding to the real-complex transition. (c) At strong disorder the non-Hermitian MBL regime corresponds to the Poisson distribution. Statistics are taken for eigenstates lying within 10% of the middle of the spectrum in the complex energy plane. The solid blue line represents the (a) GOE, (b) Ginibre, and (c) Poisson distributions. Here, the non-reciprocal hoppings are $J_L = 0.5$ and $J_R = 1.0$. The system size is $L = 16$.

system is in delocalized phase with complex energies, and it exhibits Ginibre distribution [Fig. 5(b)] $P_{\text{Gin}}^{\text{C}}(s) = cp(cs)$, which characterizes an ensemble for non-Hermitian Gaussian random matrices. Here,

$$p(s) = \lim_{N \rightarrow \infty} \left[\prod_{n=1}^{N-1} e_n(s^2) e^{-s^2} \right] \sum_{n=1}^{N-1} \frac{2s^{2n+1}}{n! e_n(s^2)} \quad (7)$$

with $e_n(x) = \sum_{m=0}^n \frac{x^m}{m!}$ and $c = \int_0^\infty ds s p(s) = 1.1429$ [66, 68]. At $W = 10$, the system is in MBL phase, and the eigenspectrum becomes real. Since the MBL phase persists even in the presence of non-reciprocal hoppings, so dubbed non-Hermitian MBL. In MBL phase, the real eigenenergy spectrum at strong disorder follows the real Poisson distribution $P_{\text{Po}}^{\text{R}}(s) = \exp(-s)$. This is evident from Fig. 5(c). The level statistics can demarcate the MBL phase by showing the characteristic level distributions.

We further consider the complex level-spacing ratio [45, 69, 70] for i th eigenvalue, which is a dimensionless complex variable and defined as

$$z_i = \frac{E_i - E_i^{\text{NN}}}{E_i - E_i^{\text{NNN}}} \equiv r_i e^{i\theta_i} \quad (8)$$

with the amplitude $r_i \equiv |z_i|$. The E_i^{NN} and E_i^{NNN} are the nearest and next-nearest neighbours of the energy level E_i in the complex plane, respectively. In general, the nearest-neighbour distance is not universal and depends on the local density of states. However, in the ratio z_i , the dependence of the local density is washed away. This ratio is an ideal diagnostic to examine the ergodicity to MBL transition. The mean level-spacing ratio $\langle r \rangle$ is obtained by the average of r_i over the energy window and number of disorder realizations. In the present study, we consider the energy window to be 10% energy eigenvalues around the center of the eigenspectrum in the complex energy plane. This choice allows us to obtain a large number of eigenvalues for the level statistics analysis and ascertain that their eigenstates share similar localization properties. The number of disorder realizations is chosen such that the total number of eigenvalues is 10^6 .

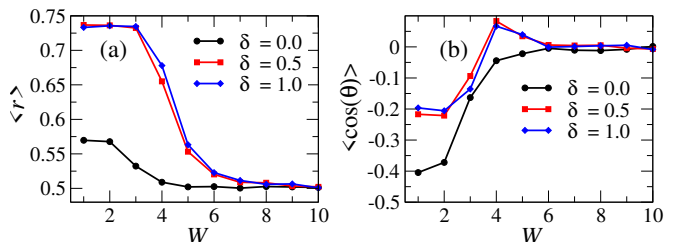


FIG. 6. (a) The average complex level-spacing ratio and (b) the cosine as a function of boundary parameters δ 's. An infinitesimal change in boundary parameter results in a change in the level statistics. We consider the system size $L = 16$. The level-spacing ratio is obtained for eigenstates lying within 10% of the middle of the eigenspectrum. The disorder average is performed for 100 realizations.

We first consider the evolution of averaged $\langle r \rangle$ as a function of W , as shown in Fig. 6(a) for $L = 16$. It is shown for non-reciprocal hoppings $J_L = 0.5$ and $J_R = 1$. For $\delta = 0$, when W is smaller, $\langle r \rangle$ attains a constant value of 0.569 [70, 71] for the GOE distribution [Fig. 5(a)]. As W increases, the value of $\langle r \rangle$ decreases and stabilizes at strong disorder. The value of $\langle r \rangle$ at strong disorder is 0.5, corresponding to real Poisson level statistics [70, 71]. Thus, even with real spectrum at $\delta = 0$, the level-spacing distribution and spacing ratio $\langle r \rangle$ can distinguish delocalization-localization transition driven by random disorder. Note that at smaller W , the reality of the eigenspectrum is due to OBC, as the time-reversal symmetric model Hamiltonian can be mapped to the corresponding Hermitian model using imaginary gauge transformation [45, 55]. We next analyze the level-statistics with non-zero δ of the generalized boundary, where the system shows complex-real transition with W . An infinitesimal coupling of both ends leads to $\langle r \rangle \approx 0.74$ [69, 72] at a smaller W for the Ginibre distribution [Fig. 5(b)]. At strong W , the $\langle r \rangle$ is 0.5. The same transition of $\langle r \rangle$ is also noted for the PBC case with $\delta = 1$. The change in value of $\langle r \rangle$ is consistent with the corresponding complex-real transition shown in Fig. 1(b).

Similarly, a variable related to the angular distributions of complex spacing ratio $\langle \cos \theta \rangle$ [69, 72] is also a single-number signature that distinguishes the different phase regimes with different level distributions. The change in the value of

$\langle \cos \theta \rangle$ as a function of W for three values of δ is shown in Fig. 6(b). For $\delta = 0$, the system exhibits GOE distributions with $\langle \cos \theta \rangle \approx -0.4$ at smaller W . As W increases, the value of $\langle \cos \theta \rangle$ increases and eventually becomes zero for Poisson statistics at strong disorder. At finite δ , $\delta = 0.5$ and $\delta = 1$, the $\langle \cos \theta \rangle \approx -0.2$ for the complex eigenenergy phase with Ginibre distribution, and the value approaches zero at strong disorder strengths. Thus, both $\langle r \rangle$ and $\langle \cos \theta \rangle$ serve as a good indicator of localization transitions with change in the level distributions. The δ and W dependence of real-complex transitions are consistent with the pertinent level-spacing distribution transitions. The critical disorder strength $W_c \approx 4$ at which the transition to localization phase occurs, agrees well with real-complex spectral transition and biorthogonal IPR [cf. Fig. 6(b), Fig. 4(b), and Fig. 1(b)].

D. Dynamical properties

We finally examine the dynamical properties of the many-body non-Hermitian system using the quantum trajectory approach [1, 73]. For a given initial state $|\psi_0\rangle$ at $t = 0$, the time evolved wave-function of non-equilibrium dynamics is

$$|\psi_t\rangle = \frac{e^{-i\mathcal{H}t/\hbar} |\psi_0\rangle}{\sqrt{\langle \psi_0 | e^{i\mathcal{H}^\dagger t/\hbar} e^{-i\mathcal{H}t/\hbar} | \psi_0 \rangle}}, \quad (9)$$

where \mathcal{H} is an effective non-Hermitian Hamiltonian governing the dynamics of non-Hermitian systems. To explore the non-equilibrium dynamics, we choose the density-wave ordered state $|101010\dots\rangle$ as an initial state where odd sites are occupied and even sites are empty. This state has routinely been prepared in experiments to investigate the localization properties of Hermitian systems [74–76].

We first examine the time dynamics of local particle density at two ends of the chain, i.e., the density at the first and last sites. The dynamics of local particle (normalized) density n_1 and n_L are presented in Fig. 7 for several cases with a set of J_L and δ . To understand the interplay of boundary sensitivity and disorder potential, it is shown for weak (a,b,c) and strong disorder (d,e,f) regimes. We begin with the evolution of n_1 and n_L at weak disorder $W = 2$. When both J_L and δ are zero, which refers to the case of an open interacting chain with unidirectional hopping, all the atoms accumulate at one end, leading to $n_1 = 1$ while $n_L = 0$ [Fig. 7(a)]. A small boundary coupling while maintaining the unidirectional hoppings results in delocalization of atoms occupying across the lattice sites. Moreover, a PBC case with $\delta = 1$ also exhibits similar behaviour [Fig. 7(a)]. A small left hopping $J_L = 0.5$ with no boundary coupling leads to accumulation of density at the first site over a long time [Fig. 7(b)]. Recall that the accumulation of atoms at the ends is due to the prevailing NHSE for OBC ($\delta = 0$) cases. The boundary coupling leads to delocalization of atoms and atoms do not accumulate at the ends of the chain despite the system being non-Hermitian due to non-reciprocal hoppings. Finally, for $J_L = 1$, the system is Hermitian, thereby even $\delta = 0$ does not accumulate the particles at the ends. And, no boundary sensitivity is seen for

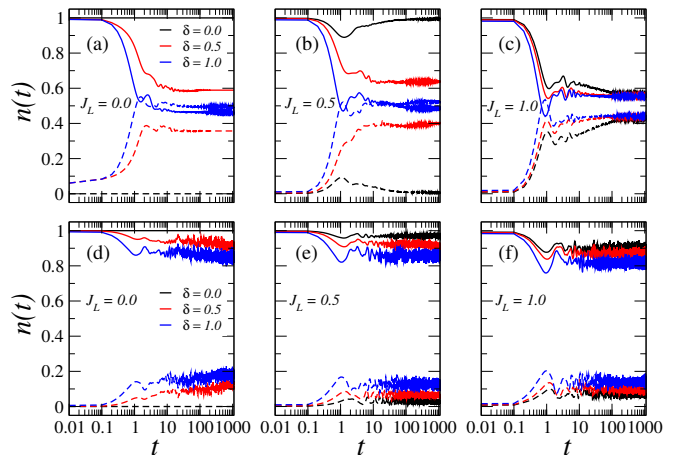


FIG. 7. The time evolution of disordered-averaged local particle density for various sets of left hopping strength and boundary parameters. This is shown for two regimes: (a,b,c) weak disorder $W = 2$ and (d,e,f) strong disorder $W = 14$. The solid lines indicate the evolution of density at the first lattice site of the chain n_1 and the corresponding dashed lines represent the density at the right end of the chain n_L . Here, the system size is $L = 16$ and $J_R = 1.0$. The density is averaged over 100 disorder realizations. The initial state is $|\psi_0\rangle = |1010\dots\rangle$.

$J_L = 1$ [Fig. 7(c)]. As the disorder strength is small, the delocalization of atoms is favoured, as apparent from the local particle densities.

We now turn to discuss the role of disorder potential. The local particle density at $W = 14$ is shown in Fig. 7(d,e,f). For a unidirectional open chain, the role of NHSE dominates, leading to full localization of atoms at the first site. However, in other cases the localization is mainly due to strong disorder, and the effects of the boundary parameter fade away. This is evident from the particle densities of non-Hermitian cases [Fig. 7(d,e)], which are similar to $J_L = 1$ (Hermitian) cases [Fig. 7(f)].

We further calculate the population imbalance, a measure of disorder-induced localization [23, 24], defined as

$$I(t) = \sum_j (-1)^j n_j. \quad (10)$$

The initial density-wave ordered state maximizes the imbalance at $t = 0$ for spinless fermions with half-filling. It is worth noting that the imbalance does not characterize the NHSE driven localization; however, it can be identified based on the local particle distributions, as discussed previously. In the followings, we investigate the experimentally accessible time evolution of disordered averaged imbalance. Fig. 8 displays the time evolution of disordered averaged imbalance for the initially prepared density-wave ordered state. The dynamics are shown for $W = 2$ (a,b,c) and $W = 14$ (d,e,f), corresponding to extended and MBL regimes, respectively. Let us recall that the memory of the initial state is lost at small disorder strength that signals the delocalization of the system and decay of imbalance. While the MBL phase is charac-

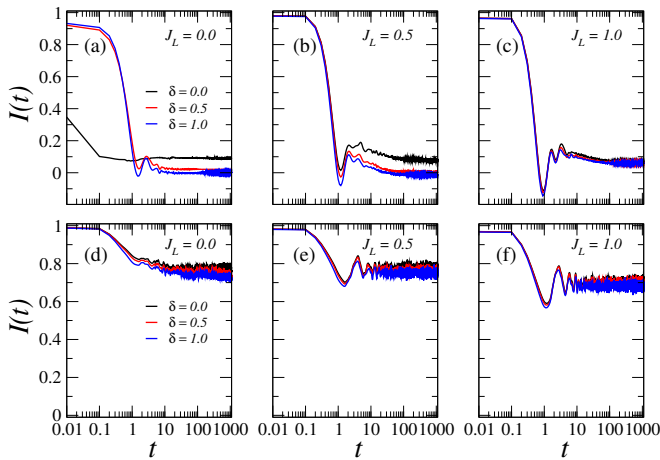


FIG. 8. The time evolution of population imbalance for various sets of left hopping strength and boundary parameters. This averaged imbalance is shown for two values of disorder strengths: (a,b,c) $W = 2$ and (d,e,f) $W = 14$. In the delocalized regime with weak disorder, $I(t)$ relaxes to zero while in the localized regime with strong disorder it saturates to a finite value characterizing (non-) Hermitian MBL. Here, the imbalance is averaged over 100 samples for system size $L = 16$. The right-hopping J_R is 1.0. The initial state is taken as $|\psi_0\rangle = |1010\dots\rangle$.

terized by a finite stationary value acquired by imbalance at long-time evolution. In the extended regime ($W = 2$), the imbalance decays to zero for all non-Hermitian and Hermitian cases considered, which implies the relaxation of the initial density profile regardless of the values of J_L and δ . However, the NHSE-driven localization in weak disorder regime is concluded for non-Hermitian OBC cases [Fig. 7(a,b)].

For strong disorder, $W = 14$, on the other hand, the imbalance saturates to a finite value, signifying the property of MBL phase. Hence, for all cases, the strong disorder leads to localization. This is consistent with the eigenspectrum [Fig. 1], where the MBL phase at strong disorder suppresses the imaginary part of the complex energies (dynamically stabilizes) and results in a real eigenspectrum.

We finally investigate the growth of the entanglement entropy to corroborate the role of hopping non-reciprocity of spinless fermions with generalized boundary. The half-chain entanglement entropy [23, 24] is defined as

$$S_E(t) = -\text{Tr}[\rho_A(t) \ln \rho_A(t)], \quad (11)$$

where the two subsystems are denoted as A and B with $\rho_A(t) = \text{Tr}_B |\psi_t\rangle \langle \psi_t|$ being the reduced density matrix of subsystem A . Here, Tr_B is the trace over degrees of freedom of subsystem B . The entanglement entropy of the initial wave-packet with non-reciprocal hopping does not spread as in the Hermitian case (in particular at weak disorder), rather slides as determined by the asymmetry in the hopping [44, 45, 48, 77, 78].

The time evolutions of disorder-averaged $S_E(t)$ at weak and strong disorder strengths are shown in Fig. 9. For unidirectional hopping under open boundaries, localization leads

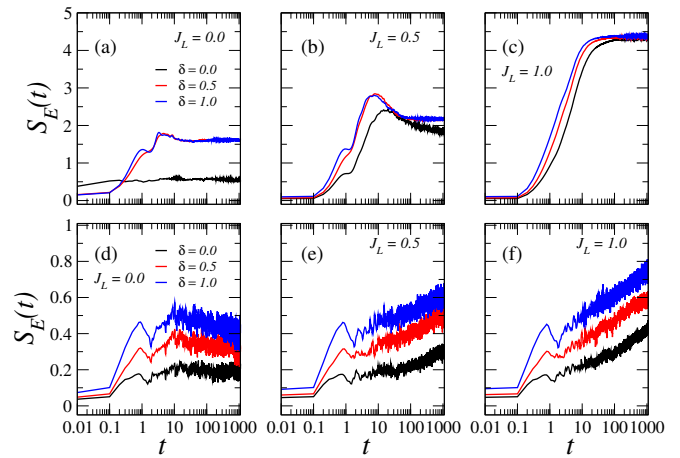


FIG. 9. The dynamics of half-chain entanglement entropy for different values of δ with (a,d) $J_L = 0$, (b,e) $J_L = 0.5$, and (c,f) $J_L = 1.0$ at weak disorder (upper panel) and strong disorder (lower panel). (a,b,c) At $W = 2$, $S_E(t)$ of an initial density-wave ordered state $|1010\dots\rangle$ first increases linearly and then saturates for reciprocal hoppings cases while it first increases and then decreases before attaining a steady value for non-reciprocal hoppings. (d,e,f) At $W = 14$, $S_E(t)$ exhibits logarithmic growth for reciprocal and non-reciprocal hoppings. The results are averaged over 100 disorder realizations for system size $L = 16$.

to lower entanglement entropy. With boundary terms, the coupling of end sites results in higher entanglement entropy and over long time it remains steady. For weak disorder, with non-reciprocal hopping the entanglement entropy decreases after a transient increase and attains a steady value over time [Fig. 9(a,b)]. For the Hermitian system, the entanglement entropy grows rapidly with time and saturates to larger values, a feature expected for the extended phase [Fig. 9(c)].

In the strong disorder regime, the entanglement entropy can be described as a logarithmic function of time, compatible with the characteristic of MBL phase [Fig. 9(e,f)]. Hence, the entropy of entanglement of initially separable density-wave ordered states grows logarithmically in time after initial transients signify MBL with non-reciprocal hopping under generalized boundary.

IV. CONCLUSIONS

We solved exactly the non-Hermitian Hatano-Nelson model of interacting spinless fermions and investigated the interplay of localization phenomena due to boundary sensitivity and disorder potential. An infinitesimal variation in the boundary term leads to spectrum and localization transitions in a one-dimensional fermionic chain. The random disorder potential washes away the real-complex transitions due to the prevailing non-Hermitian MBL. We further analyze IPR with its biorthogonal version and level statistics to reveal the coincidence of real-complex spectral transition with localization transition. Moreover, the emergence of real spectra due to infinitesimal change in boundary parameter even at weaker dis-

order is attributed to NHSE, which is identified using nearest-neighbour level spacing distributions. Finally, the two localization phenomena, namely NHSE and MBL, are distinguished by the non-equilibrium dynamics of local particle densities and population imbalance. The time evolution of densities demonstrates the atomic localizations at the first site while that of imbalance shows relaxation to a finite value. This confirms NHSE-driven localization with non-reciprocal hopping. While the steady imbalance and logarithmic growth of entanglement entropy at strong disorder validate the features of MBL in interacting non-Hermitian systems. With the recent advancement in engineering non-reciprocal hopping by reservoir coupling, we believe that our findings will inspire the

realization of localization transitions in non-Hermitian disordered systems.

ACKNOWLEDGMENTS

We thank Yi-Cheng Wang, Jih-Shih You, and H. H. Jen for valuable discussions. K.S. acknowledges support from the Science and Engineering Research Board, Department of Science and Technology, Government of India through Project No. SRG/2023/001569.

-
- [1] Y. Ashida, Z. Gong, and M. Ueda, Non-Hermitian physics, *Adv. Phys.* **69**, 249 (2020).
- [2] E. J. Bergholtz, J. C. Budich, and F. K. Kunst, Exceptional topology of non-Hermitian systems, *Rev. Mod. Phys.* **93**, 015005 (2021).
- [3] S. Weidemann, M. Kremer, S. Longhi, and A. Szameit, Topological triple phase transition in non-Hermitian floquet quasicrystals, *Nature* **601**, 354 (2022).
- [4] K. Kawabata, T. Numasawa, and S. Ryu, Entanglement phase transition induced by the non-Hermitian skin effect, *Phys. Rev. X* **13**, 021007 (2023).
- [5] Y. Sun, T. Shi, Z. Liu, Z. Zhang, L. Xiao, S. Jia, and Y. Hu, Fractional quantum zeno effect emerging from non-Hermitian physics, *Phys. Rev. X* **13**, 031009 (2023).
- [6] Y. Yang, B. Yang, G. Ma, J. Li, S. Zhang, and C. T. Chan, Non-abelian physics in light and sound, *Science* **383**, eadf9621 (2024).
- [7] Z. Gong, Y. Ashida, K. Kawabata, K. Takasan, S. Higashikawa, and M. Ueda, Topological phases of non-Hermitian systems, *Phys. Rev. X* **8**, 031079 (2018).
- [8] C. Li, R. Yang, X. Huang, Q. Fu, Y. Fan, and F. Zhang, Experimental demonstration of controllable \mathcal{PT} and anti- \mathcal{PT} coupling in a non-Hermitian metamaterial, *Phys. Rev. Lett.* **132**, 156601 (2024).
- [9] J. Li, A. K. Harter, J. Liu, L. de Melo, Y. N. Joglekar, and L. Luo, Observation of parity-time symmetry breaking transitions in a dissipative floquet system of ultracold atoms, *Nat. Commun.* **10**, 855 (2019).
- [10] S. Lapp, J. Ang'ong'a, F. A. An, and B. Gadway, Engineering tunable local loss in a synthetic lattice of momentum states, *New J. Phys.* **21**, 045006 (2019).
- [11] Z. Ren, D. Liu, E. Zhao, C. He, K. K. Pak, J. Li, and G.-B. Jo, Chiral control of quantum states in non-Hermitian spin-orbit-coupled fermions, *Nat. Phys.* **18**, 385 (2022).
- [12] Q. Liang, D. Xie, Z. Dong, H. Li, H. Li, B. Gadway, W. Yi, and B. Yan, Dynamic signatures of non-Hermitian skin effect and topology in ultracold atoms, *Phys. Rev. Lett.* **129**, 070401 (2022).
- [13] R. Rosa-Medina, F. Ferri, F. Finger, N. Dogra, K. Kroeger, R. Lin, R. Chitra, T. Donner, and T. Esslinger, Observing dynamical currents in a non-Hermitian momentum lattice, *Phys. Rev. Lett.* **128**, 143602 (2022).
- [14] Z. Dong, H. Li, T. Wan, Q. Liang, Z. Yang, and B. Yan, Quantum time reflection and refraction of ultracold atoms, *Nat. Photonics* **18**, 68 (2024).
- [15] S. Imhof, C. Berger, F. Bayer, J. Brehm, L. W. Molenkamp, T. Kiessling, F. Schindler, C. H. Lee, M. Greiter, T. Neupert, and R. Thomale, Topological-circuit realization of topological corner modes, *Nat. Phys.* **14**, 925 (2018).
- [16] B. Liu, Y. Li, B. Yang, X. Shen, Y. Yang, Z. H. Hang, and M. Ezawa, Experimental observation of non-Hermitian higher-order skin interface states in topological electric circuits, *Phys. Rev. Res.* **5**, 043034 (2023).
- [17] L. Lu, J. D. Joannopoulos, and M. Soljačić, Topological photonics, *Nat. Photonics* **8**, 821 (2014).
- [18] A. B. Khanikaev and G. Shvets, Two-dimensional topological photonics, *Nat. Photonics* **11**, 763 (2017).
- [19] Y. Yang, Y. F. Xu, T. Xu, H.-X. Wang, J.-H. Jiang, X. Hu, and Z. H. Hang, Visualization of a unidirectional electromagnetic waveguide using topological photonic crystals made of dielectric materials, *Phys. Rev. Lett.* **120**, 217401 (2018).
- [20] J. Lu, W. Deng, X. Huang, M. Ke, and Z. Liu, Non-Hermitian topological phononic metamaterials, *Adv. Mater.* **n/a**, 2307998 (2023).
- [21] Z. Yang, F. Gao, X. Shi, X. Lin, Z. Gao, Y. Chong, and B. Zhang, Topological acoustics, *Phys. Rev. Lett.* **114**, 114301 (2015).
- [22] H. Xue, Y. Yang, and B. Zhang, Topological acoustics, *Nat. Rev. Mater.* **7**, 974 (2022).
- [23] F. Alet and N. Laflorencie, Many-body localization: An introduction and selected topics, *C. R. Phys.* **19**, 498 (2018).
- [24] D. A. Abanin, E. Altman, I. Bloch, and M. Serbyn, Colloquium: Many-body localization, thermalization, and entanglement, *Rev. Mod. Phys.* **91**, 021001 (2019).
- [25] P. Sierant, M. Lewenstein, A. Scardicchio, L. Vidmar, and J. Zakrzewski, Many-body localization in the age of classical computing, *Rep. Prog. Phys.* (2024).
- [26] M.-H. L. Xiujuan Zhang, Tian Zhang and Y.-F. Chen, A review on non-Hermitian skin effect, *Adv. Phys.: X* **7**, 2109431 (2022).
- [27] W. Gou, T. Chen, D. Xie, T. Xiao, T.-S. Deng, B. Gadway, W. Yi, and B. Yan, Tunable nonreciprocal quantum transport through a dissipative aharonov-bohm ring in ultracold atoms, *Phys. Rev. Lett.* **124**, 070402 (2020).
- [28] W. Wang, M. Hu, X. Wang, G. Ma, and K. Ding, Experimental realization of geometry-dependent skin effect in a reciprocal two-dimensional lattice, *Phys. Rev. Lett.* **131**, 207201 (2023).
- [29] X. Zhang, Y. Tian, J.-H. Jiang, M.-H. Lu, and Y.-F. Chen, Observation of higher-order non-Hermitian skin effect, *Nat. Commun.* **12**, 5377 (2021).

- [30] F. K. Kunst, E. Edvardsson, J. C. Budich, and E. J. Bergholtz, Biorthogonal bulk-boundary correspondence in non-Hermitian systems, *Phys. Rev. Lett.* **121**, 026808 (2018).
- [31] S. Yao and Z. Wang, Edge states and topological invariants of non-Hermitian systems, *Phys. Rev. Lett.* **121**, 086803 (2018).
- [32] D. Halder, S. Ganguly, and S. Basu, Properties of the non-Hermitian ssh model: role of \mathcal{PT} symmetry, *J. Phys. Condens. Matter* **35**, 105901 (2022).
- [33] K. Kawabata, M. Sato, and K. Shiozaki, Higher-order non-Hermitian skin effect, *Phys. Rev. B* **102**, 205118 (2020).
- [34] D. S. Borgnia, A. J. Kruchkov, and R.-J. Slager, Non-Hermitian boundary modes and topology, *Phys. Rev. Lett.* **124**, 056802 (2020).
- [35] Z. Gu, H. Gao, H. Xue, J. Li, Z. Su, and J. Zhu, Transient non-Hermitian skin effect, *Nat. Commun.* **13**, 7668 (2022).
- [36] R. Lin, T. Tai, L. Li, and C. H. Lee, Topological non-Hermitian skin effect, *Front. Phys.* **18**, 53605 (2023).
- [37] T. Yoshida, S.-B. Zhang, T. Neupert, and N. Kawakami, Non-Hermitian mott skin effect, *Phys. Rev. Lett.* **133**, 076502 (2024).
- [38] X.-R. Ma, K. Cao, X.-R. Wang, Z. Wei, Q. Du, and S.-P. Kou, Non-Hermitian chiral skin effect, *Phys. Rev. Res.* **6**, 013213 (2024).
- [39] C.-X. Guo, C.-H. Liu, X.-M. Zhao, Y. Liu, and S. Chen, Exact solution of non-Hermitian systems with generalized boundary conditions: Size-dependent boundary effect and fragility of the skin effect, *Phys. Rev. Lett.* **127**, 116801 (2021).
- [40] S.-B. Zhang, M. M. Denner, T. c. v. Bzdušek, M. A. Sentef, and T. Neupert, Symmetry breaking and spectral structure of the interacting Hatano-Nelson model, *Phys. Rev. B* **106**, L121102 (2022).
- [41] D.-W. Zhang, Y.-L. Chen, G.-Q. Zhang, L.-J. Lang, Z. Li, and S.-L. Zhu, Skin superfluid, topological Mott insulators, and asymmetric dynamics in an interacting non-Hermitian Aubry-André-Harper model, *Phys. Rev. B* **101**, 235150 (2020).
- [42] C.-Z. Lu and G. Sun, Many-body entanglement and spectral clusters in the extended hard-core bosonic Hatano-Nelson model, *Phys. Rev. A* **109**, 042208 (2024).
- [43] Z.-C. Liu, K. Li, and Y. Xu, Dynamical transition due to feedback-induced skin effect, *Phys. Rev. Lett.* **133**, 090401 (2024).
- [44] R. Hamazaki, K. Kawabata, and M. Ueda, Non-Hermitian many-body localization, *Phys. Rev. Lett.* **123**, 090603 (2019).
- [45] K. Suthar, Y.-C. Wang, Y.-P. Huang, H. H. Jen, and J.-S. You, Non-Hermitian many-body localization with open boundaries, *Phys. Rev. B* **106**, 064208 (2022).
- [46] J. Mák, M. Bhaseen, and A. Pal, Statics and dynamics of non-Hermitian many-body localization, *Commun. Phys.* **7**, 92 (2024).
- [47] L.-J. Zhai, S. Yin, and G.-Y. Huang, Many-body localization in a non-Hermitian quasiperiodic system, *Phys. Rev. B* **102**, 064206 (2020).
- [48] Y.-C. Wang, K. Suthar, H. H. Jen, Y.-T. Hsu, and J.-S. You, Non-Hermitian skin effects on thermal and many-body localized phases, *Phys. Rev. B* **107**, L220205 (2023).
- [49] S. Cheng, X. Feng, W. Chen, N. A. Khan, and G. Xianlong, Stable real-energy spectral dynamics with topological transitions and non-Hermitian many-body localization, *Phys. Rev. B* **109**, 174209 (2024).
- [50] H.-Z. Li, X.-J. Yu, and J.-X. Zhong, Non-Hermitian stark many-body localization, *Phys. Rev. A* **108**, 043301 (2023).
- [51] J. Liu and Z. Xu, From ergodicity to many-body localization in a one-dimensional interacting non-Hermitian stark system, *Phys. Rev. B* **108**, 184205 (2023).
- [52] N. Hatano and D. R. Nelson, Localization transitions in non-Hermitian quantum mechanics, *Phys. Rev. Lett.* **77**, 570 (1996).
- [53] N. Hatano and D. R. Nelson, Vortex pinning and non-Hermitian quantum mechanics, *Phys. Rev. B* **56**, 8651 (1997).
- [54] N. Hatano and D. R. Nelson, Non-Hermitian delocalization and eigenfunctions, *Phys. Rev. B* **58**, 8384 (1998).
- [55] N. Hatano and H. Obuse, Delocalization of a non-Hermitian quantum walk on random media in one dimension, *Ann. Phys.* **435**, 168615 (2021).
- [56] W. Visscher, Localization of electron wave functions in disordered systems, *J. Non-Cryst. Solids* **8-10**, 477 (1972), amorphous and Liquid Semiconductors.
- [57] F. Evers and A. D. Mirlin, Fluctuations of the inverse participation ratio at the anderson transition, *Phys. Rev. Lett.* **84**, 3690 (2000).
- [58] Y.-X. Xiao and C. T. Chan, Topology in non-Hermitian chern insulators with skin effect, *Phys. Rev. B* **105**, 075128 (2022).
- [59] P. Wang, L. Jin, and Z. Song, Non-Hermitian phase transition and eigenstate localization induced by asymmetric coupling, *Phys. Rev. A* **99**, 062112 (2019).
- [60] O. Bohigas, M. J. Giannoni, and C. Schmit, Characterization of chaotic quantum spectra and universality of level fluctuation laws, *Phys. Rev. Lett.* **52**, 1 (1984).
- [61] T. Guhr, A. Müller-Groeling, and H. A. Weidenmüller, Random-matrix theories in quantum physics: common concepts, *Phys. Rep.* **299**, 189 (1998).
- [62] M. L. Mehta, *Random Matrices* (Elsevier, 2004).
- [63] F. Haake, *Quantum Signatures of Chaos* (Springer, 2013).
- [64] R. Hamazaki, K. Kawabata, N. Kura, and M. Ueda, Universality classes of non-Hermitian random matrices, *Phys. Rev. Res.* **2**, 023286 (2020).
- [65] S. Shivam, A. De Luca, D. A. Huse, and A. Chan, Many-body quantum chaos and emergence of ginibre ensemble, *Phys. Rev. Lett.* **130**, 140403 (2023).
- [66] R. Grobe, F. Haake, and H.-J. Sommers, Quantum distinction of regular and chaotic dissipative motion, *Phys. Rev. Lett.* **61**, 1899 (1988).
- [67] J. Ginibre, Statistical ensembles of complex, quaternion, and real matrices, *J. Math. Phys.* **6**, 440 (1965).
- [68] H. Markum, R. Pullirsch, and T. Wettig, Non-Hermitian random matrix theory and lattice qcd with chemical potential, *Phys. Rev. Lett.* **83**, 484 (1999).
- [69] L. Sá, P. Ribeiro, and T. c. v. Prosen, Complex spacing ratios: A signature of dissipative quantum chaos, *Phys. Rev. X* **10**, 021019 (2020).
- [70] Z. Xiao, K. Kawabata, X. Luo, T. Ohtsuki, and R. Shindou, Level statistics of real eigenvalues in non-Hermitian systems, *Phys. Rev. Res.* **4**, 043196 (2022).
- [71] T. Peron, B. M. F. de Resende, F. A. Rodrigues, L. d. F. Costa, and J. A. Méndez-Bermúdez, Spacing ratio characterization of the spectra of directed random networks, *Phys. Rev. E* **102**, 062305 (2020).
- [72] A. M. García-García, L. Sá, and J. J. M. Verbaarschot, Symmetry classification and universality in non-Hermitian many-body quantum chaos by the sachdev-ye-kitaev model, *Phys. Rev. X* **12**, 021040 (2022).
- [73] A. J. Daley, Quantum trajectories and open many-body quantum systems, *Adv. Phys.* **63**, 77 (2014).
- [74] M. Schreiber, S. S. Hodgman, P. Bordia, H. P. Lüschen, M. H. Fischer, R. Vosk, E. Altman, U. Schneider, and I. Bloch, Observation of many-body localization of interacting fermions in a quasirandom optical lattice, *Science* **349**, 842 (2015).
- [75] T. Kohlert, S. Scherg, X. Li, H. P. Lüschen, S. Das Sarma, I. Bloch, and M. Aidelsburger, Observation of many-body lo-

- calization in a one-dimensional system with a single-particle mobility edge, *Phys. Rev. Lett.* **122**, 170403 (2019).
- [76] S. Scherg, T. Kohlert, P. Sala, F. Pollmann, B. Hebbe Madhusudhana, I. Bloch, and M. Aidelsburger, Observing non-ergodicity due to kinetic constraints in tilted fermi-hubbard chains, *Nat. Commun.* **12**, 4490 (2021).
- [77] T. Orito and K.-I. Imura, Unusual wave-packet spreading and entanglement dynamics in non-Hermitian disordered many-body systems, *Phys. Rev. B* **105**, 024303 (2022).
- [78] T. Orito and K.-I. Imura, Entanglement dynamics in the many-body Hatano-Nelson model, *Phys. Rev. B* **108**, 214308 (2023).